On solitary wave diffraction by multiple, in-line vertical cylinders

Neill, Douglas R.; Hayatdavoodi, Masoud; Ertekin, R. Cengiz

Published in:
Nonlinear Dynamics

DOI:
10.1007/s11071-017-3923-1

Publication date:
2018

Document Version
Peer reviewed version

Nonlinear Dynamics manuscript No.
(will be inserted by the editor)

On Solitary Wave Diffraction by Multiple, In-line Vertical Cylinders

Douglas R. Neill
Masoud Hayatdavoodi
R. Cengiz Ertekin

Received: date / Accepted: date

Abstract The interaction of solitary waves with multiple, in-line vertical cylinders is investigated. The fixed cylinders are of constant circular cross-section and extend from the sea floor to the free surface. In general, there are N of them lined in a row parallel to the incoming wave direction. Both the nonlinear, generalized Boussinesq and the Green-Naghdi shallow-water wave equations are used. A boundary-fitted curvilinear coordinate system is employed to facilitate the use of the finite-difference method on curved boundaries. The governing equations and boundary conditions are transformed from the physical plane onto the computational plane. These equations are then solved in time on the computational plane that contains a uniform grid and by use of the successive over relaxation method and a second-order finite-difference method to determine the horizontal force and overturning moment on the cylinders. Resulting solitary wave forces from the nonlinear Green-Naghdi and the Boussinesq equations are presented, and the forces are compared with the experimental data when available.

D. R. Neill
National Optical Astronomy Observatory, 950 N Cherry Ave., Tucson, AZ 85719, USA

M. Hayatdavoodi
Civil Engineering Department, School of Science and Engineering, University of Dundee, Dundee DD1 4HN, UK
E-mail: mhayatdavoodi@dundee.ac.uk

R.C. Ertekin
Guest Professor, College of Shipbuilding Engineering, Harbin Engineering University, Harbin, China

Keywords Solitary wave · multiple inline vertical circular cylinders · wave force and moment · Boussinesq equations · Green-Naghdi equations

1 Introduction

Many marine structures are built on vertical cylinders; consequently, the determination of the forces which are a result of the wave-cylinder interaction is an important problem in ocean engineering. However, very few studies have considered nonlinear shallow-water wave equations to investigate solitary- and cnoidal-wave diffraction by vertical cylinders and calculated the forces and moments acting on it.

We consider here the interaction of solitary waves with fixed, multiple inline vertical cylinders of constant circular cross section. The cylinders extend from the seafloor to the free surface, and the still-water depth is held constant. Different shallow-water wave equations can produce different solitary waves, and may describe the flow field differently, and thereby can lead to different wave loads. Both the generalized Boussinesq (gB) (Wu (1981)) and the Green-Naghdi (GN) (Green and Naghdi (1977)) Level I equations are used to solve numerically the initial-boundary-value problem to obtain the horizontal forces and overturning moments on multiple cylinders in shallow water.

The linearized potential problem of wave diffraction by a single vertical cylinder was solved by MacCamy and Fuchs (1954) for an ideal fluid. The infinite depth solution of the same problem was obtained earlier by Havelock (1940). Scattering of waves for very long wave length (solitary wave) by a cylindrical object (island) was first solved by Omer and Hall (1949).

Only few investigations of nonlinear effects in the time domain exist compared with the linear ones. Isaacson (1983) studied the interaction of a solitary wave with an isolated cylinder by an approximate method by using the linear boundary conditions although the solitary wave problem has to be nonlinear. Isaacson and Cheung (1992) used a second-order time-domain method to investigate this problem. These studies showed good agreement between the numerical predictions and experimental data. Wang et al. (1992) used a generalized Boussinesq model to investigate the nonlinear effects of wave-cylinder interaction on hydrodynamic forces. Their investigation indicated that linear equations may produce wave forces that are 40% less than those predicted by nonlinear equations. Yang and Ertekin (1992) used the boundary-element method to solve the fully nonlinear diffraction problem to investigate the

diffraction of a solitary wave and Stokes waves by a vertical circular cylinder in finite water depth; they solved Laplace's equation for an ideal fluid subject to the exact boundary conditions to determine nonlinear wave diffraction and loading. Neill and Ertekin (1997) studied the diffraction of solitary waves by a vertical cylinder in shallow waters and presented some preliminary results. More recently, Ghadimi et al. (2012) studied the diffraction of linear waves by a floating, vertical circular cylinder and solved Laplace's equations by use of the strip theory.

Most of the previous works have been extended to wave diffraction by isolated cylinders, and the influence of neighboring cylinders is more limited. McIver and Evans (1984) estimated the wave forces on a group of fixed, vertical cylinders by solving Laplace's equation subject to linear boundary conditions, and by use of an approximated method to account for the effect of neighboring cylinders in the array. Similar approach was followed by Linton and Evans (1990) to determine wave loads on an array of cylinders; they solved the linear equations exactly, closely following a method suggested earlier by Spring and Monkmeyer (1974). Other studies on wave diffraction by an array of vertical cylinders include Malenica et al. (1999); Kagemoto et al. (2002); Han et al. (2015); Kamath et al. (2015); Barlas (2012). Solitary wave interaction with a group of vertical cylinders is studied by Mo and Liu (2009); Mo (2010) by use of numerical models based on the Navier-Stokes and Euler's equations. Kudeih et al. (2010) conducted laboratory experiments to study random wave loads on an array of vertical cylinders in shallow water.

Our goal in this paper is to study the problem of diffraction of solitary waves by multiple-inline vertical cylinders in shallow water, by use of the Level I GN equations and the generalized Boussinesq equations, and discuss the nonlinearity effect on the wave loads on the cylinders. Our objectives are (i) to develop two models based on these well-known nonlinear, shallow-water wave equations, (ii) to study the flow field and the wave impact on multiple inline cylinders, including the effects of the neighbouring cylinders, and (iii) to compare the results of these models with each other, and with the existing data.

We first introduce the nonlinear shallow-water wave equations that we use and formulate the initial-boundary-value problem and discuss the wavemaker solutions of these equations. This is followed by the discussion on grid generation, where we reformulate the problem in the computational plane after transforming the problem from the physical plane. We then discuss the numer-

ical method used and finally present the results obtained for multiple in-line cylinders. Both the predicted forces and moments on the vertical cylinders are compared with the experimental data and predictions by others whenever they are available, see e.g., Yates and Wang (1994). Finally, results are discussed with an emphasis on how these two sets of shallow-water equations can predict the flow field around multiple, in-line vertical cylinders.

2 Theory

A Cartesian coordinate system, whose origin is on the upwave or entrance boundary where the numerical wave maker is located, is used. In this three-dimensional system, the $x-$direction is along the line of symmetry, which also is perpendicular to the incident wave crest-line. The $y-$direction is parallel to the entrance boundary, and the $z-$direction is vertical, with positive z up, see Fig 1. It is assumed that the vertical cylinders have constant, circular cross section and the still-water depth, h, is held constant. The problem is symmetric with respect to the line that passes through the in-line cylinders center and is perpendicular to the wave crest-line. Since the problem is symmetric, only one half of the physical region needs to be considered. The physical problem is modeled as an initial-boundary-value problem. In Fig. 1, the upwave boundary is where the numerical wavemaker is located and the downwave boundary is the "open" boundary or absorbing boundary to prevent possible reflections as much as possible. On the symmetry, far wall and the cylinder boundaries, the normal component of the fluid velocities must vanish but we allow the tangential component as the fluid is assumed to be inviscid in this work.

2.1 Shallow-water wave equations

The solitary wave scattering, horizontal forces and overturning moment on the vertical, in-line cylinders are calculated in time by solving either the GN or gB equations. In this section, the governing equations and assumptions made in developing the theoretical models are discussed.

2.1.1 The Green-Naghdi (GN) Equations

The GN equations use the assumption that the fluid is incompressible and homogeneous. In this study, the fluid is assumed inviscid, although this is not

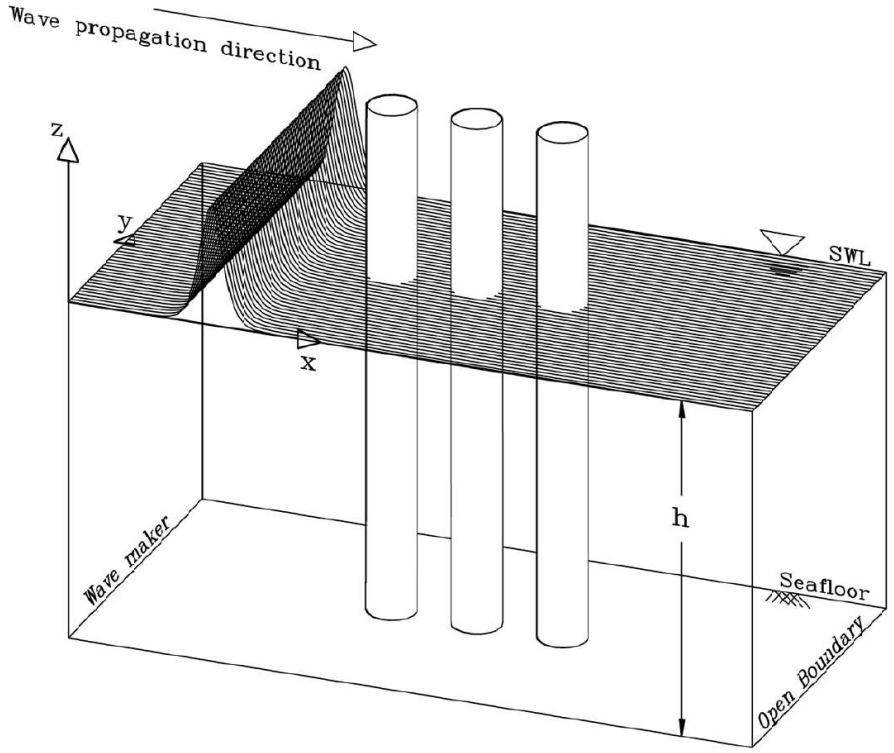

Fig. 1 Schematic of the numerical wave tank, showing different boundaries discussed in the text, and showing three in-line cylinders. Not to scale.

a requirement for the GN equations in general, see Green and Naghdi (1984). The derivation of the equations does not require the flow to be irrotational, therefore, the velocity potential does not exist. Investigations of these equations were made by Green and Naghdi (1976a,b); Ertekin (1984); Ertekin et al. (1986); Ertekin (1988); Shields and Webster (1988); Demirbilek and Webster (1992); Ertekin et al. (2014), among others.

Unlike the Boussinesq-class equations, the GN equations do not follow from a perturbation expansion. The order of error, therefore, cannot be defined. The range of applicable wave lengths and heights must be determined by comparisons with experimental data. The kinematic and dynamic free-surface conditions are satisfied exactly. However, the conservation equations are satisfied exactly in the depth averaged sense only. Ertekin (1984) obtained rather a classical form of the GN equations (see also Ertekin et al. (1986)). The GN equations can be specialized to our case by setting the pressure on the top

surface of the fluid sheet ($\hat{p}$) to atmospheric, and further assume that it is negligible, and by setting the water depth to constant ($\alpha = 0$) in the original equations given by Ertekin (1984):

$$\zeta_t + \boldsymbol{\nabla} \cdot \{(h+\zeta)\boldsymbol{V}\} = 0\,, \tag{1}$$

$$\dot{u} + g\zeta_x = -\frac{1}{3}\{2\zeta_x\ddot{\zeta} + (h+\zeta)\ddot{\zeta}_x\}\,, \tag{2}$$

$$\dot{v} + g\zeta_y = -\frac{1}{3}\{2\zeta_y\ddot{\zeta} + (h+\zeta)\ddot{\zeta}_y\}\,, \tag{3}$$

where h is the constant water depth, g is the gravitational acceleration, ζ is the free surface elevation measured from the still-water level, and $\boldsymbol{\nabla}$ is the gradient vector operator, $\boldsymbol{\nabla} = (\partial/\partial x)\boldsymbol{e_1} + (\partial/\partial y)\boldsymbol{e_2}$, and $\boldsymbol{V} = u\boldsymbol{e_1} + v\boldsymbol{e_2}$ is the particle velocity vector on the horizontal plane as these are assumed to not depend on the vertical z coordinate in the Level I GN equations. In higher level GN equations, however, they would depend on the z coordinate, see e.g., Shields and Webster (1988); Zhao et al. (2014a, 2015). $\boldsymbol{e_1}$ and $\boldsymbol{e_2}$ are the unit base vectors in the x and y directions, respectively. It is understood that the subscripts denote differentiation with respect to them. The superposed dot denotes the material time derivative, i.e., for any physical quantity f, we have $\dot{f} = f_t + uf_x + vf_y$. A double superposed dot denotes the second material time derivative. Note that Eq. (1) is a statement of conservation of mass and Eqs. (2) and (3) are statements of conservation of linear momentum and director momentum (moment of momentum) combined, in the x and y directions, respectively.

The following dimensionless variables are used in this study by selecting (ρ, g, h) as a dimensionally independent set:

$$\bar{t} = \frac{t}{h}\sqrt{gh}, \quad \bar{F} = \frac{F}{\rho g h^2 R}, \quad \bar{M} = \frac{M}{\rho g h^3 R}, \quad \bar{P} = \frac{P}{\rho g h}, \tag{4}$$

where the bars represent the dimensionless quantities, and ρ is the mass density, F is the horizontal force on the cylinder, M is the overturning moment with respect to the sea floor, P is the pressure, and R is the cylinder radius. Any quantity whose dimension is length is scaled by h and any quantity which has the dimension of velocity is scaled by $\sqrt{gh}$. The same nondimensionalization is used for the gB equations and the linear equations and the bars over the physical quantities will be dropped for convenience unless otherwise stated.

A close look at Eqs. (2) and (3) shows that they involve the second order time derivative of the surface elevation. By combining the definition of mate-

rial derivative with the continuity equation, Eq. (1), a new equation for the second derivative of ζ can be obtained. This procedure results in removing the difficulties associated with the presence of the time derivatives of the surface elevation on the right-hand sides of Eqs. (2) and (3). As discussed by Qian (1994), this is accomplished by first isolating ζ_t in Eq. (1) and then substituting it into the first material derivative of ζ. As a result, the first material derivative of ζ no longer contains a partial derivative with respect to time, t, i.e., $\dot{\zeta} = -\boldsymbol{\nabla} \cdot [(h+\zeta)\boldsymbol{V}] + \boldsymbol{V} \cdot \boldsymbol{\nabla}\zeta$. The local time derivative of the surface elevation, ζ, is again removed from its second material derivative to obtain $\ddot{\zeta} = (h+\zeta)[(u_x+v_y)^2 - (u_{tx}+v_{ty}) - u(u_{xx}+v_{xy}) - v(u_{xy}+v_{yy})]$. Substituting these into Eqs. (2) and (3) produces a set of component equations that do not contain the second derivatives with respect to time, and this is a very significant step to efficiently and accurately obtain the numerical solutions of these equations. The dimensionless form of the GN equations, Eqs. (1)-(3), after eliminating the time derivatives of ζ from the right-side of the momentum equations can be obtained as

$$\zeta_t = -\zeta_x u - \zeta_y v - (\zeta+1)\left(u_x + v_y\right) , \tag{5}$$

$$\begin{aligned} &u_t - (\zeta+1)\,\zeta_x\left(u_{xt}+v_{yt}\right) - \frac{1}{3}(\zeta+1)^2\left(u_{xxt}+v_{xyt}\right) = -\zeta_x - uu_x - vu_y \\ &- (\zeta+1)\,\zeta_x\left[(u_x+v_y)^2 - u\left(u_{xx}+v_{xy}\right) - v\left(u_{xy}+v_{yy}\right)\right] - \frac{1}{3}(\zeta+1)^2 \cdot \\ &\cdot \left(\left(u_x+2v_y\right)\left(u_{xx}+v_{xy}\right) - v_x\left(u_{xy}+v_{yy}\right) - u\left(u_{xxx}+v_{xxy}\right) - v\left(u_{xxy}+v_{xyy}\right)\right) , \end{aligned} \tag{6}$$

$$\begin{aligned} &v_t - (\zeta+1)\,\zeta_y\left(u_{xt}+v_{yt}\right) - \frac{1}{3}(\zeta+1)^2\left(u_{xyt}+v_{yyt}\right) = -\zeta_y - uv_x - vv_y \\ &- (\zeta+1)\,\zeta_y\left[(u_x+v_y)^2 - u\left(u_{xx}+v_{xy}\right) - v\left(u_{xy}+v_{yy}\right)\right] - \frac{1}{3}(\zeta+1)^2 \cdot \\ &\cdot \left[\left(2u_x+v_y\right)\left(u_{xy}+v_{yy}\right) - v_y\left(u_{xx}+v_{xy}\right) - u\left(u_{xxy}+v_{xyy}\right) - v\left(u_{xyy}+v_{yyy}\right)\right] . \end{aligned} \tag{7}$$

2.1.2 The generalized Boussinesq (gB) Equations

We use the generalized Boussinesq equations based in the form derived by Wu (1981) for constant water depth and for zero atmospheric pressure. We give here the dimensionless form of these equations after we use Eq. (4) and remove

the bars over the quantities:

$$\zeta_t + \boldsymbol{\nabla} \cdot \{(1+\zeta)\,\boldsymbol{\nabla}\phi\} = 0\,, \tag{8}$$

$$\phi_t + \frac{1}{2}||\boldsymbol{\nabla}\phi||^2 + \zeta = \frac{1}{3}\boldsymbol{\nabla}\phi_t\,, \tag{9}$$

where ϕ is the layer-mean velocity potential. These equations assume an incompressible and inviscid fluid. The use of the layer-mean velocity potential, also requires the assumption of irrotationality of the flow. The bottom no-flux condition as well as the kinematic and dynamic free-surface conditions are satisfied approximately in the derivation of the gB equations.

The first gB equation, Eq. (8), is simply the continuity equation and represents the conservation of mass statement. The second equation, Eq. (9), follows from the momentum equation, and is obtained using perturbation methods. Therefore, the conservation of momentum is satisfied only approximately. The error is of order $(\alpha\epsilon^4, \alpha^2\epsilon^2)$ as shown by Wu (1981), where $\alpha = A/h$, $\epsilon = h/L$, where A is the wave amplitude and L is the wave length. The two parameters, α and ϵ, represent the nonlinear and dispersive behaviors of waves, respectively. For the gB equations, both parameters are assumed to be small, $O(\alpha) = O(\mu^2) < 1$, where $\mu = kh = 2\pi\epsilon$. The gB equations are most applicable when the Ursell parameter, $U_r = \alpha/\mu^2$, is of $O(1)$.

The gB equations are not used here in the common form given by Eqs. (8) and (9) (as was done by Ertekin et al. (1990)) mainly for reasons of convenience in programming. The layer-mean velocity potential is instead eliminated from the equations by using the definition of the velocity potential. The layer-mean velocity potential is the average of the 3-D velocity potential over the depth of the fluid. This is in contrast to the 3-D velocity potential which represents the flow state at a specific point in time. The Eqs. (8) and (9) then are written in nondimensional component form as

$$\zeta_t + \boldsymbol{\nabla} \cdot \{(1+\zeta)\,\boldsymbol{V}\} = 0\,, \tag{10}$$

$$\dot{u} = u_t + uu_x + vu_y + \zeta_x = \frac{1}{3}\left(u_{xx} + u_{yy}\right)_t = \frac{1}{3}\Delta u_t\,, \tag{11}$$

$$\dot{v} = v_t + uv_x + vv_y + \zeta_y = \frac{1}{3}\left(v_{xx} + v_{yy}\right)_t = \frac{1}{3}\Delta v_t\,, \tag{12}$$

where Δ is the 2-D Laplacian on the horizontal plane. Clearly, this set of equations are simpler than the GN equations, (5)-(7), as there are less number of terms and derivatives involved.

2.2 Initial and Boundary Conditions

The initial conditions are chosen to correspond to a quiescent fluid, i.e., $\zeta(x, y, 0) = u(x, y, 0) = 0$. Therefore, the velocities and surface elevations are initially set to zero at which time the incident waves are located outside the computational domain on the upwave side. The boundary conditions along the line of symmetry, the surface of the cylinder, and the far wall, are the no-flux condition. This line of symmetry is along the wave propagation direction. The symmetry axis acts like a rigid surface, therefore, no flow is allowed through this surface. The normal velocity (v) therefore is equal to zero. The downwave boundary is an open boundary. The waves must be absorbed by this boundary without reflection. At the upwave boundary, the wavemaker solution, will be presented in subsequent sections for the solitary wave.

The sea-floor no-flux condition, as well as the kinematic and dynamic free-surface conditions, are accounted for directly in the derivations of the gB (approximately) and GN (exactly) equations, and therefore, they are not given here. See Green and Naghdi (1976a) and Wu (1981) for details on how the boundary conditions are embedded into the GN and gB equations, respectively.

Although we use a large computational domain for greater accuracy, it is necessary to use an absorption boundary on the downwave side. Previous works of Wu and Wu (1982) and Ertekin (1984) showed that the relatively simple Orlanski's condition with constant phase speed $c = \pm\sqrt{gh}$ prevents significant reflections from the open-boundary. We use this open-boundary condition here which reads

$$\Omega_t + c\Omega_x = 0, \tag{13}$$

where Ω may be $\zeta(x, t)$ or $u(x, t)$ at the downwave boundary.

It is noted that after the solitary wave has completely entered into the computational domain through the upwave boundary, the upwave boundary converts to the Orlanski condition, Eq. (13) (see e.g., Ertekin et al. (1986)) to absorb any reflected waves, similar to the downwave boundary.

We note that with regards to the implementation of the open boundary condition, Eq. (13), the use of the incident wave speed on the downwave open boundary instead of the linear wave speed provides superior wave absorption. Since this boundary needs to absorb supercritical solitary waves, the introduction of the incident wave speed in the Orlanski condition allows this radiation boundary to absorb the remainder of the incident wave after it had traversed

the entire domain. The upwave boundary where the wavemaker is located need to absorb any reflections due to the diffraction of solitary waves, and therefore, the linear long-wavelength limit, $c = \sqrt{gh}$, is used for the wave speed in the Orlanski condition on the upwave boundary. We monitored the wave elevations at various numerical wave gauges and observed that the open-boundary conditions work well with minimum amount of reflections.

2.3 Wave-maker solutions

There are different types of solitary wave solutions. Some shallow-water equations provide an analytic solitary-wave solution (as in the GN equations used here) and others need to be calculated numerically (as in the gB equations used here).

2.3.1 GN Solitary Wavemaker

An analytic solitary wave solution of the the GN Level I equations can be found in Green and Naghdi (1976a), and in Ertekin (1984), who has studied a number of constrained domain problems in shallow water involving solitons. The dimensional solitary-wave solution of the GN equations is given by[1]

$$\zeta(x') = A sech^2\left(\tau \;\; x'\right) , \tag{14}$$

where

$$\tau = \sqrt{\frac{3A}{4h^2(A+h)}} . \tag{15}$$

and A is the amplitude of the solitary wave measured from the still-water level and is given by

$$A = \frac{c^2}{g} - h \quad \text{or} \quad \frac{c}{\sqrt{gh}} = \sqrt{1 + \frac{A}{h}}, \tag{16}$$

where c is the speed (critical or supercritical, or the depth Froude number $Fr = U/\sqrt{gh} \geq 1$) of the wave, h is the constant water depth and $x' = x - x_0 - Ut$, where x_0 is the midpoint of the solitary wave at time $t = 0$. The horizontal velocity can be determined from the conservation of mass equation in the moving coordinates, $u = c\zeta/(1+\zeta)$. Hayatdavoodi and

[1] This solution is the same as given by Rayleigh (1876).

Ertekin (2015c) presented a closed-form of the GN solitary wave horizontal and vertical velocities as

$$u(x',0) = \sqrt{g(A+h)}\frac{A\,sech^2\left(\tau x'\right)}{h + A\,sech^2\left(\tau x'\right)}\,, \tag{17}$$

$$w(x',z,0) = \frac{z+h}{h + A\,sech^2\left(\tau x'\right)}\left(2A\,sech^2\left(\tau x'\right)\tanh\left(\tau x'\right)\right)\left(\sqrt{g(A+h)} - u\right)\,. \tag{18}$$

Since the solitary wave in theory has an infinite length, it is not necessary to modulate it as long as it is located well to the left of the upwave boundary at time $t = 0$. Discussion on the steady, solitary-wave solution of high-level GN equations can be found in Zhao et al. (2014b).

2.3.2 gB Solitary Wavemaker

The solitary wave solution of the gB equations uses the same numerically determined wave solution used by Qian (1994); Roddier and Ertekin (1999) (see also Teng and Wu (1992)). This solution is found by eliminating the time derivatives from the gB equations by converting them to the moving or wave coordinates. The gB equations then can be combined into a single differential equation:

$$\zeta_x^2 = \frac{6}{Fr^2}(1+\zeta)^4\ln(1+\zeta) + \left(2 + \frac{6}{Fr^2}\right)(1+\zeta)^4 - \left(3 + \frac{6}{Fr^2}\right)(1+\zeta^3) + (1+\zeta)\,, \tag{19}$$

where $Fr = c/\sqrt{gh}$ is the depth Froude number and c is the dimensional wave celerity as before. The wave profile then is determined iteratively from Eq. (19). The amplitude, A, of the soliton is input into Eq. (19) as the initial value of ζ at the wave crest. We then use the 4th-order Runge-Kutta method to determine the slope for other values of x' to determine $\zeta(x')$ at the next step $x'_{i+1} = x'_i + \Delta x'$. This process is repeated until the wave profile is completed, also see e.g., Roddier (1994); Neill (1996) for more details.

2.4 Force and Moment Calculations

2.4.1 GN Equations

Ertekin (1984) provided closed-form relations for the integrated pressure (over the water depth) and the bottom pressure (on the seafloor). These relations are given by

$$P_I(x,y,t) = \frac{1}{6}(1+\zeta)^2\left(2\ddot{\zeta}+3\right), \quad p(x,y,t) = \frac{1}{2}(1+\zeta)\left(\ddot{\zeta}+2\right), \tag{20}$$

respectively.

The total wave force on the cylinder is obtained by numerically integrating the pressure P_I around the circumference of the cylinder in the direction of the unit normal vector on the cylinder. The horizontal force component is then obtained by taking its $x-$component.

A difficulty exists in determining the resulting overturning moment for the GN equations. There is neither an expression for the moment nor an expression for the pressure as a function of depth that would allow the calculation of the moment. This difficulty is overcome here by assuming that the variation of the total pressure is linear with depth (equal to zero on the free surface and equal to the sea floor pressure on the bottom). This assumption is in close agreement with the pressure distribution predicted by the gB equations. This will be further discussed in the Results and Discussion Section. The error associated to the assumption of linear variation of pressure can be estimated, and indeed it is very small, as we will discuss later in this section.

The depth-varying pressure reads

$$P(x,y,z,t) = \frac{1}{2}(\zeta - z)\left(\ddot{\zeta}+2\right). \tag{21}$$

Therefore, to determine the equation for the overturning moment with respect to the sea floor, Eq. (21) is multiplied by the moment arm, and then integrated over the depth:

$$M_I(x,y,t) = \int_{-1}^{\zeta}(1+z)\,P(z)\,dz = \frac{1}{12}(1+\zeta)^3\left(\ddot{\zeta}+2\right). \tag{22}$$

The moment acting on the cylinder can then be determined numerically by integrating the $x-$component of M_I around the circumference of the cylinder. See, e.g., Hayatdavoodi and Ertekin (2015b,a), for an approach to determine

the wave-induced loads on horizontal objects by use of the Level I GN equations.

To determine the error of using Eq. (21) in approximating the pressure distribution in the z direction, we integrate $P(x, y, z, t)$ of Eq. (21) over the water depth:

$$P_{IL}(x, y, t) = \int_{-1}^{\zeta} P(x, y, z, t)\, dz = \frac{1}{4}(1+\zeta)^2 \left(\ddot{\zeta} + 2\right). \tag{23}$$

The percent error, ϵ, made by the assumption of linearly-varying total pressure along the water column is then determined by comparing the integrated (linearly-varying) pressure, P_{IL}, with the integrated pressure of the GN equations given by Eq. (20):

$$\epsilon = \left|\frac{P_I - P_{IL}}{P_I}\right| \times 100 = \left|\frac{\ddot{\zeta}}{4\ddot{\zeta} + 6}\right| \times 100. \tag{24}$$

Although Eq. (24) determines the error produced by the integrated pressure, it also is a reasonable estimate of the error produced by the moment equation (22). This error is determined for every node along the cylinder boundary and then an average is calculated. This average is then used as an approximate error value in the moment calculations as discussed later in Section 5.3.

2.4.2 gB Equations

Unlike the GN equations, the pressure as a function of depth is provided by the gB equations in terms of the layer-mean potential, see Wu (1981). However, we write the gB pressure equation in dimensionless velocity form:

$$P(z) = \zeta - z + \left(z + \frac{1}{2}z^2\right) \boldsymbol{\nabla} \cdot \boldsymbol{V}_t. \tag{25}$$

To facilitate the determination of the force, we integrate Eq. (25) over the water column and obtain

$$P_I = \frac{1}{2}(1+\zeta)^2 + \frac{1}{6}(1+\zeta)\left(\zeta^2 + 2(\zeta - 1)\right) \boldsymbol{\nabla} \cdot \boldsymbol{V}. \tag{26}$$

Multiplying Eq. (25) by the moment arm and integrating over the depth gives the expression for the overturning moment (about the y axis) with respect

to the seafloor:

$$M_I = \frac{1}{6}(1+\zeta)^3 + \frac{1}{8}(1+\zeta)^2\left((1+\zeta)^2 - 2\right)\boldsymbol{\nabla}\cdot\boldsymbol{V}_t\,. \tag{27}$$

Finally, the integrated pressure and moment, P_I and M_I, are numerically integrated around the circumference of the cylinder in the direction of the unit normals on the cylinder to determine the horizontal force in the x direction and the overturning moment about the y axis, respectively.

3 Grid Generation

To facilitate the use of finite-difference methods to solve shallow water wave equations in the presence of irregular boundaries, numerical grid generation is used in this study. The use of numerical grid generation allows the inclusion of irregular boundaries conveniently by mapping the physical domain into a rectangular computational domain. The grid chosen for the computational domain is both regular and rectangular. This is not a requirement for the use of the grid-generation transformation system. It does, however, significantly reduce the complexity of the computations. The present study uses an elliptical generation technique in a connected 2-D region. Since the problem contains a symmetry axis, only one half of the region needs to be analyzed. Therefore, the grid system does not need to have re-entrant boundaries in either the physical or transformed plan.

The use of elliptical grid generation technique has been described extensively by, for example, Thompson et al. (1977). In this technique, a one-to-one mapping is developed between the physical plane and the computational plane by use of the Laplace equation. A uniform computational grid system with unit interval spacings is used in the solution of all the governing equations. This greatly simplifies the use of finite-difference methods. The minimization of the Euler integral ensures a one-to-one mapping. Details on the transformation of the governing equations as used in this work can be found in Qian (1988); Ertekin et al. (1990).

4 Numerical Method

We use the finite-difference method to solve the partial differential equations that govern the fluid motion. The difference equations are found through the

use of the second-order central difference formulas in space. To use the difference equations along the boundaries, a fictitious point method is used. For example, along any boundary $x = x_1$, the equation for the first derivative would be

$$f'(x_1) = \frac{f(x_0) - f(x_2)}{2\Delta x} + O(\Delta x^2). \tag{28}$$

However, since x_0 is outside of the boundary, $f(x_0)$ is undefined. A fictitious value for $f(x_0)$ is found through a parabolic approximation: $f_0 = 3f_1 - 3f_2 + f_3$. By combining this equation with Eq.(28), a new equation is produced for the first derivative along the boundary:

$$f'(x_1) = \frac{-3f(x_1) + 4f(x_2) - f(x_3)}{2\Delta x} + O(\Delta x^2). \tag{29}$$

This method can be used to produce equations for all the derivatives along the boundaries, see Roddier (1994); Roddier and Ertekin (1999) for more details.

We use the time marching technique known as the modified Euler method, see e.g., Burden and Faires (1985). This two-step method has second-order accuracy. This method was also used successfully by Ertekin (1984); Ertekin et al. (1986); Roddier and Ertekin (1999); Hayatdavoodi and Ertekin (2015c), among others, in the solution of the GN and gB equations in 2-D.

The Successive Over-Relaxation (SOR) iterative method is used to solve the transformed forms of three sets of equations: GN Eqs. (5), (6), (7); and gB Eqs. (10), (11), (12). Two modifications are made to this method to improve the computational efficiency. Normally, the solution for u and v at the last time step is used as the initial guess for the next time step. In this analysis, however, the initial guess is extrapolated from the last two time steps using $u_{k+1}(i,j) - 2u_k(i,j) - u_{k-1}(i,j)$ and $v_{k+1}(i,j) - 2v_k(i,j) - v_{k-1}(i,j)$, where k is the time counter. Shown by Roddier and Ertekin (1999), this method reduces the number of SOR iterations by more than 40%. The second modification is to alternate the starting point and order of the iterations. Instead of always starting at $i = 1, j = 1$, the starting point is alternated between the four corners of the computational domain, $A(i = 1, j = 1)$, $D(i = 1, j = n)$, $E(i = m, j = 1)$ and $F(i = m, j = n)$. This technique also reduced the number of iterations.

The analysis carried out here requires filtering to remove numerical noise and ensure stability as pointed out by Ertekin et al. (1986). Much of this noise is the result of the central-difference scheme. When insufficient filtering is applied, the results become unstable. The third-order filtering by itself does

not provide sufficient stability. Our studies show that a combination of the five- (2nd order) and seven-point (3rd order) linear filtering schemes used here was developed by Shapiro (1975) and proved adequate to ensure stability. This includes the use of a third-order filtering in the direction normal to the prevailing wave crests, the ξ direction, and a second-order filtering parallel to the wave crests, the η direction. This does not modify the shape of the incoming waves. The filtering formulas that we use are given by

$$\begin{aligned} f_j &= \frac{1}{16}\left(-f_{j-2}+4f_{j-1}+10f_j+4f_{j+1}-f_{j-2}\right), \\ f_i &= \frac{1}{64}\left(-f_{i-3}-6f_{i-2}+15f_{i-1}+44f_i+15f_{i+1}-6f_{i+2}+f_{i+3}\right), \end{aligned} \tag{30}$$

where f is a generic variable that can represent ζ, u or v.

5 Error Monitoring

5.1 Conservation of Mass

To monitor the accuracy of the numerical solutions, the change in the mass due to numerical errors is determined following the approach used by Qian (1994); Roddier (1994). Conservation of mass is satisfied exactly for both the Green-Naghdi and the Boussinesq equations. Except for mass passing through the upstream or downstream boundaries, any change in mass is due to numerical errors. The Green-Naghdi equations exactly satisfy the conservation of momentum in the depth averaged sense, while the Boussinesq equations satisfy the momentum conservation approximately. Therefore, to monitor the numerical errors, the change in mass is chosen (preferred) here over the change in momentum or mechanical energy.

The total excess mass inside the physical domain (M), at a specific time, is determined by numerically integrating over the water column and over the surface area of the physical domain:

$$M = \int_A (1+\zeta)\, dA. \tag{31}$$

The mass flow through the open boundaries is determined by integrating over these boundaries:

$$dm_{US} = \int_{US} (1+\zeta)\,(\mathbf{v}.\mathbf{n})\,ds\,, \tag{32}$$

$$dm_{DS} = \int_{DS} (1+\zeta)\,(\mathbf{v}.\mathbf{n})\,ds\,, \tag{33}$$

where, dm_{US} is the mass flow through the upstream boundary, and dm_{DS} is the mass flow through the downstream boundary. These boundaries are normal to the y-axis, therefore, the dot product of the velocity vector ($\mathbf{v}$) and the unit normal ($\mathbf{n}$) is simply the horizontal velocity in the x-direction (u). Therefore, Eqs. (32) and (33) are simplified to

$$dm_{US} = \int_{US} (1+\zeta)\,uds\,, \tag{34}$$

$$dm_{DS} = \int_{DS} (1+\zeta)\,uds\,. \tag{35}$$

These equations must also be integrated over time to determine the total loss or gain of mass across these boundaries.

$$dm_{US} = \int_t \int_{US} (1+\zeta)\,(\mathbf{v}.\mathbf{n})\,dsdt'\,, \tag{36}$$

$$dm_{DS} = \int_t \int_{DS} (1+\zeta)\,(\mathbf{v}.\mathbf{n})\,dsdt'\,, \tag{37}$$

where both the temporal and spacial integrations are performed numerically using Simpsons rule.

The total change in mass (dM_e) which is a result of numerical errors is found through the following relationship:

$$dM_e = M - M_0 - dM_{US} + dM_{DS}\,, \tag{38}$$

where M_0 is the initial total mass which is equal to ρV_D, where V_D is the volume of the quiescent body of fluid. The percent change in mass due to numerical errors can then be calculated through

$$M_E = \frac{dM_e}{M_0} * 100(\%)\,. \tag{39}$$

The percent change in mass, as a function of time, is determined for each case. Some sample values for M_E for both the Green-Naghdi and the Boussi-

nesq solitary waves are given in Neill (1996). The maximum values of -0.20% for the solitary wave are found to be the typical mass excess for the cases studied here. In general, the solitary waves produce negative changes in mass. The Green-Naghdi equations and the Boussinesq equations produced similar mass change results.

5.2 Stability Conditions

It was shown by Ertekin (1984) through a Von Neumann stability analysis of the linearized Green-Naghdi equations that Δt must be less than Δx for stability. This is equivalent to satisfying the Courant condition, which is accomplished by setting $\Delta t < \Delta x$ or Δy. Since the Boussinesq and Green-Naghdi equations both linearize to the same equations, see Ertekin (1984), this stability analysis applies equally well to the Boussinesq equations. The nominal values of Δt, Δx and Δy used are 0.20, $0.25h$ and $0.33h$, respectively. Consequently, this criteria is not violated in the grid systems that are used in this study.

5.3 Green-Naghdi Moment Error

As discussed in Section 2.4, to determine the moment resulting from the Green-Naghdi equations, a linear pressure distribution over the water depth is assumed. The error caused by this assumption is determined through Eq. (24). This error is determined for each cylinder and in every case analyzed. Examples of these errors are given for the Green-Naghdi solitary, and cnoidal, waves in Neill (1996). It is shown that the moment error for the solitary wave cases is less than 1.8%. This is primarily caused by the very large amplitude of the solitary wave case considered ($A = 0.5h$). Given the simplifying assumption made about the pressure distribution over the z direction, the error is reasonably small.

6 Numerical Setup

The principle configuration for solitary waves in this study is a $4.0h$ diameter cylinder and a $0.5h$ wave amplitude, unless otherwise is mentioned. This

configuration is used in many solitary wave cases and is chosen primarily to facilitate the comparison with other studies. Moreover, the $0.5h$ wave amplitude is at the practical limit of use for the gB equations. According to Mei (1989), these equations are applicable for $O(A) < 1$. This limit is a result of the assumptions that led to the derivation of these equations. Although the GN equations do not have an explicit limit, they must, nevertheless, have similar implicit limitations. Any such limitations of the GN equations must be judged by comparison with experiments.

The $4.0h$ cylinder diameter is also a convenient and reasonable size. This size is large enough to produce significant diffraction, and is easily modeled numerically. Smaller cylinders would require finer grids for the same accuracy and viscous forces may become important. A larger diameter cylinder would require a larger domain. Clearly, the latter two factors would increase the computational time significantly.

The domain used includes a $20h$ distance from the upwave boundary to the first cylinder surface, a $20h$ distance from the last cylinder surface to the downwave boundary and a $20h$ distance from the far wall to the symmetry axis. It will be shown later that this domain is large enough to avoid problems of wave interactions at the boundaries that affect the resulting forces and moments on the cylinders.

The nominal (dimensionless) grid sizes used in this domain are $\Delta x = 0.25$ and $\Delta y = 0.33$. These sizes are small enough to adequately model the surface displacements and large enough to not require excessive CPU (central processing unit) time. To insure stability, the time step must be smaller than the grid size as discussed before. Therefore, the time step is chosen as $\Delta t = 0.2$.

7 Results and Discussion

Results of the GN and the gB equations for solitary wave interaction with vertical cylinders are presented and discussed in this section. We will first start by solitary wave interaction with a single cylinder and compare the results of the theoretical models with the existing laboratory measurements and other theories. This is then followed by results and discussion on solitary wave interaction with two and three in-line vertical cylinders. We note that in this study, and for the two and three cylinder configurations, all cylinders have the same diameter.

7.1 Comparisons: Solitary Wave Interaction with a Single Cylinder

A comparison of time series of solitary wave force on a vertical cylinder, calculated by the GN and the gB equations versus the laboratory experiments of Yates and Wang (1994) is shown in Fig.2. In this case, the circular cylinder diameter is $D = 3.18h$, and the wave amplitude is $A = 0.44h$. The wave force and time are given in dimensionless form following Eq. (4).

In this comparison, both the GN and the Boussinesq models have slightly overestimated the maximum and minimum values of the wave force, although the GN equations are in closer agreement with the laboratory experiments. Such discrepancy between the results of the GN and the Boussinesq models with the laboratory measurements of Yates and Wang (1994) was previously reported by Neill and Ertekin (1997), and was also observed by Yates and Wang (1994) who compared results of their Boussinesq model with their own laboratory measurements.

The laboratory experiments are conducted in a very small scale, and in water depth of $h = 4cm$. The viscous effected, neglected in the inviscid theoretical models discussed here, may be noticeable at such small scales. Such effects play a significant role on the slight differences between results. Moreover, the theoretical models are executed for the nominal wave amplitude of $A = 0.44h$ corresponding to $A = 1.76cm$. Any small difference between the wave amplitudes of the laboratory measurements and the theoretical models would result in some differences in the wave forces. In the absence of any presentation of the undisturbed solitary waves in Yates and Wang (1994), this is possibly another reason of the discrepancy, particularly noting that the traveling speed of the wave in the laboratory is smaller than the two theories; see the differences of the time of the force troughs in Fig.2. Recall from Eq. (16) that solitary wave speed increases with larger wave amplitudes.

A comparison of the time series of the solitary wave force on a vertical cylinder calculated by the GN and the gB models, with existing theoretical solutions is shown in Fig. 3. In this case, the cylinder diameter is $D = 4.0h$ and the wave amplitude is $A = 0.5h$. In this comparison, the results of the GN and the Boussinesq models are in good agreement with other theoretical solutions, and fall between the BEM solution of Yang and Ertekin (1992) and the gB model of Wang et al. (1992). The peak of the solitary wave force of the GN model is in very close agreement with the BEM results, and is slightly smaller than the Boussinesq results.

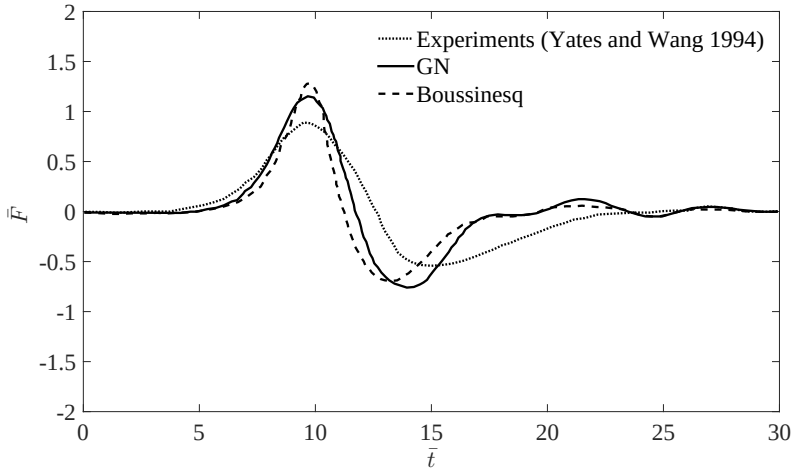

Fig. 2 Comparison of time series of solitary wave force on a single, vertical cylinder calculated by the GN and gB equations versus the laboratory experiments of Yates and Wang (1994). $A = 0.44h$ and $D = 3.18h$.

The analytical solution of Isaacson (1978) of wave force on the vertical cylinder has underestimated the force amplitude when compared to other solutions. In contrast, the Boussinesq model results of Wang et al. (1992) over estimates the force amplitude when compared to other results. Such overestimation appears to be due to the error associated to the mesh and the numerical solution of the equations. As discussed by Neill (1996), the wave run-up on the cylinder, and consequently the peak of the solitary wave forces, would increase if grid repulsion is not used, as in the Boussinseq model of Wang et al. (1992). The use of the grid repulsion improves the grid line orthogonality along the curved boundaries. The larger wave run-up in the Wang et al. (1992) model, also causes a larger wave reflection, resulting in smaller force trough when compared with the Boussinesq model discussed here, see Fig. 3.

Further results and discussion of the GN and the gB models on solitary wave interaction with a single cylinder can be found in Neill and Ertekin (1997).

7.2 Solitary Wave Interaction with Two Cylinders

The two cylinder solitary wave case also uses the same $4.0h$ diameter cylinder and $0.5h$ wave amplitude used before. This allows direct comparison with

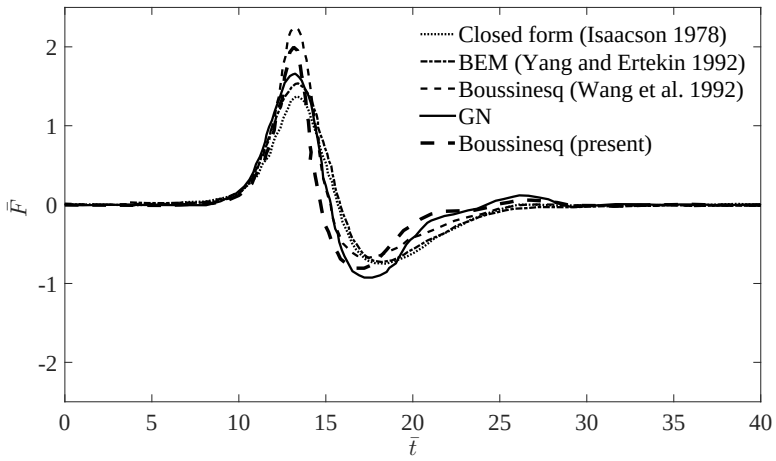

Fig. 3 Comparison of time series of solitary wave force on a single, vertical cylinder calculated by the GN and gB equations and existing theoretical solutions. $A = 0.5h$ and $D = 4.0h$.

Wang and Jiang (1994) who used the gB equations to study this configuration. Various spacings are used between the cylinders. In this section, the spacings used are $0.50D$, $0.75D$, $1.00D$, $2.00D$ and $3.00D$, where D, the diameter of the cylinder, is the same for both cylinders. The spacing between the two cylinders is measured as the closest distance between the cylinders. This is the same definition for spacing used by Wang and Jiang (1994). These spacings correspond to distances from the wave maker to the second cylinder center of $28h$, $29h$, $30h$, $34h$ and $38h$, respectively. Wang and Jiang (1994) also used the spacings of $0.0D$ and $0.25D$. For the $S = 0.0D$ spacing, the cylinder surfaces are in direct contact with each other.

Sample snapshots of the solitary wave surface elevations, calculated by the gB and the GN equations, are shown in Figs. 4 and 5, respectively. The resultant forces and moments in our study are shown in Figs. 6 and 7 for the gB equations and in Figs. 8 and 9. for the GN equations. Note that, the single cylinder results are also shown in these figures.

In general, the GN equations predict less shielding than the gB equations. Shielding is the reduction in force and moment on the downwave cylinder caused by the interaction of the waves on the upwave cylinder. The gB equations predict a greater run-up on the first cylinder. This greater run-up causes more significant wave reflection and therefore there is a greater reduction in

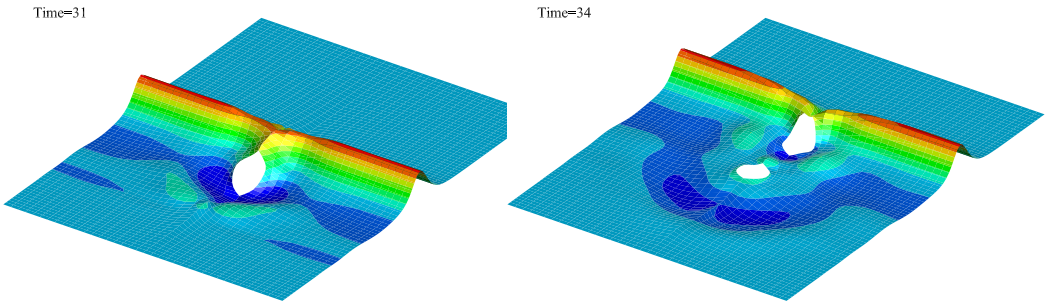

Fig. 4 3-D snapshots of solitary wave surface elevation around two cylinders, calculated by the gB equations, $S = 1.0D, D = 4.0h$ and $H = 0.5h$.

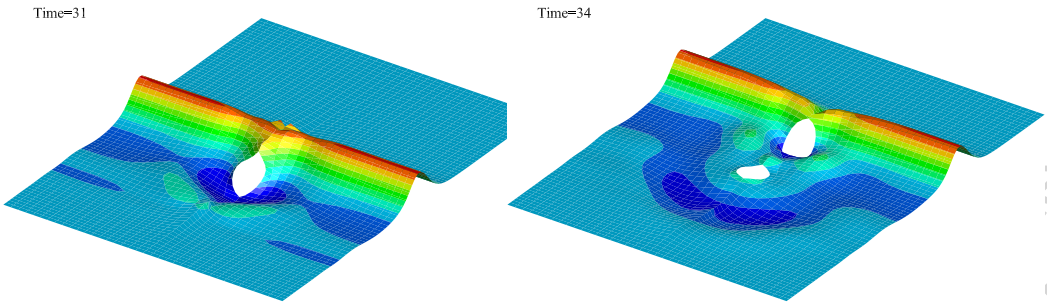

Fig. 5 3-D snapshots of solitary wave surface elevation around two cylinders, calculated by the GN equations, $S = 1.0D, D = 4.0h$ and $H = 0.5h$.

the wave amplitude downwave of the cylinder, and hence a greater reduction in the resulting force on the downwave cylinder.

The shielding described by Wang and Jiang (1994) is similar to the shielding found in this study. After the wave impacts the first cylinder, a 3-dimensional back-scattered wave emerges in front of the first cylinder. The primary wave deforms behind the first cylinder with a reduced wave amplitude. Therefore, the wave runup, force and moment are less for the second cylinder than the

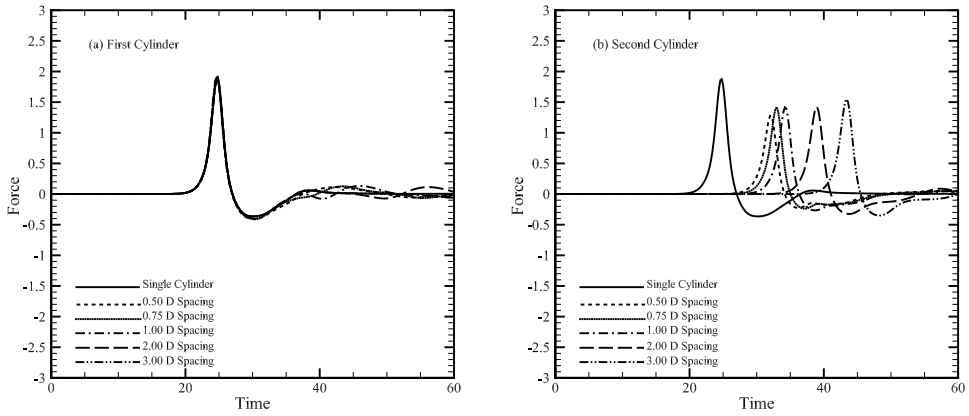

Fig. 6 Solitary wave forces on the (a)first and (b)second cylinder, for the two cylinder case, calculated by the gB equations, $H = 0.5h, D = 4.0h$.

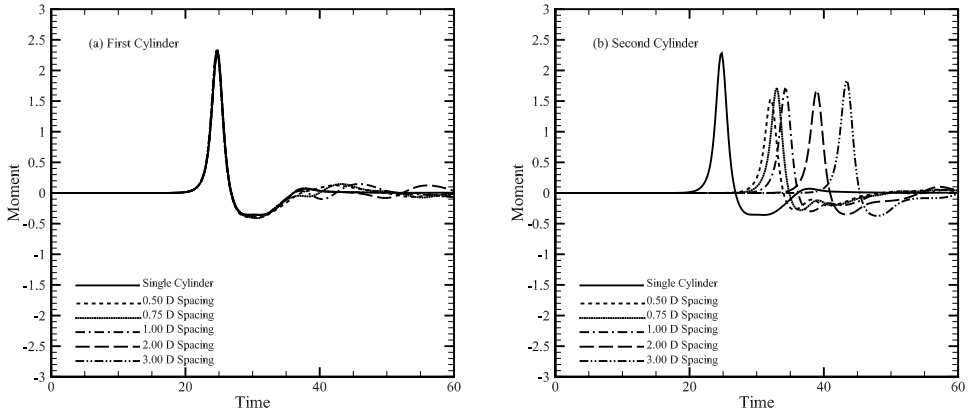

Fig. 7 Solitary wave moment on the (a)first and (b)second cylinder, for the two cylinder case, calculated by the gB equations, $H = 0.5h, D = 4.0h$.

first. The gB solution in this study consistently produces similar result to that of Wang and Jiang (1994), see Figs. 6 and 7. The small differences may be due to the lack of boundary orthogonality control in Wang and Jiang (1994) which causes the peak force value to be over-predicted. In both this study and Wang and Jiang (1994), the maximum force on the first cylinder is unaffected by the presence of the second cylinder. The maximum force on the second cylinder ($F_{max} = 1.60$), calculated by the gB equations in this study, is 21.6%

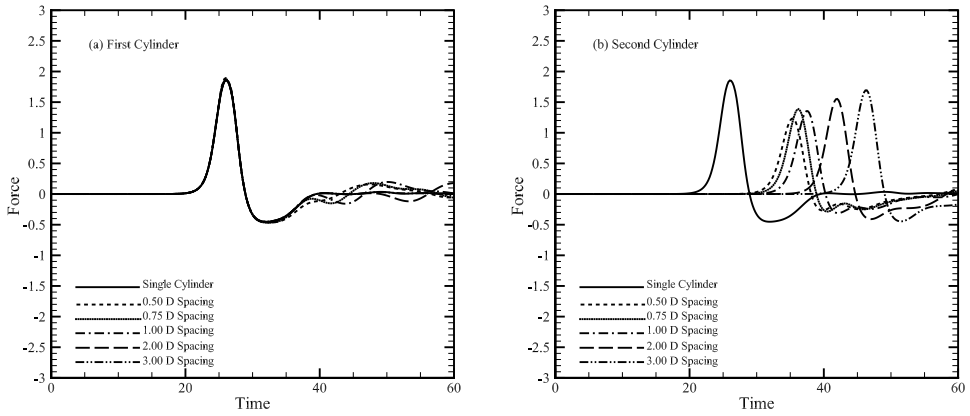

Fig. 8 Solitary wave forces on the (a)first and (b)second cylinder, for the two cylinder case, calculated by the GN equations, $H = 0.5h, D = 4.0h$.

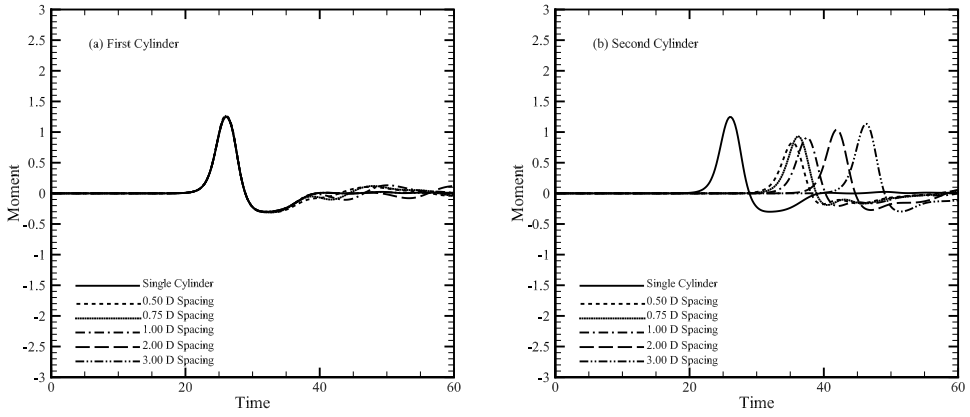

Fig. 9 Solitary wave moment on the (a)first and (b)second cylinder, for the two cylinder case, calculated by the GN equations, $H = 0.5h, D = 4.0h$.

smaller than that of the single cylinder case because of the presence of the first cylinder; the second cylinder is effectively shielded by the first cylinder.

In general, smaller distances between the cylinders leads to greater shielding and more force and moment reduction on the second cylinder as expected. A notable exception to this rule is the spacings of $0.0D$ and $0.25D$ used in Wang and Jiang (1994). For these spacings, there is a noticeable increase in both the maximum wave force on the second cylinder and the maximum neg-

ative wave force on the first cylinder. This effect is also seen to a much smaller extent in the $0.5D$ spacing as shown in Figs. 6-8. The $0.0D$ and $0.25D$ spacings are not included in this work. It is concluded that sufficient boundary orthogonality control could not be produced for these small spacings to produce more accurate results. It is unclear how much the forces of the $0.0D$ and $0.25D$ spacings causes calculated in Wang and Jiang (1994) were affected by any numerical error. The overturning moment on the cylinders show similar behaviour to the wave-induced horizontal force.

The GN solution shows much less reduction in the maximum force (F_{max}= 1.48, 11.4% reduction) for the second cylinder, see Figs. 8 and 9. In general, the shielding does become more pronounced, and the resulting force and moment on the second cylinder are reduced as the cylinder spacing is reduced. It should be noted that, although the force and moment reduction on the second cylinder is less for the GN solution, the actual force and moment on the second cylinder is still less than the equivalent force for the gB case. This is the result of the greater force and moment in the gB case, for the single cylinder.

7.3 Solitary Wave Interaction with Three Cylinders

For this case, a third cylinder with identical dimensions is added to the row. The $0.5h$ wave amplitude and $4.0h$ cylinder diameter are used again. The spacing between the second and third cylinders is equal to the spacing between the first and second cylinders. These spacings, $0.50D$, $0.75D$, $1.00D$, $2.00D$ and $3.00D$ correspond to distances from the wave maker to the third cylinder center of $34h$, $36h$, $38h$, $46h$ and $54h$, respectively.

Samples of the solitary wave surface elevations for the three cylinder case, calculated by the gB and the GN equations, are shown in Figs. 10 and 11, respectively. The resulting forces and moments from the gB equations are shown in Figs. 12, 13 and 14. The resulting forces and moments from the GN equations are shown in Figs. 15, 16 and 17.

For both the gB and the GN equations, the forces and moment on the first and second cylinders of the three-cylinder case, see Figs. 12-17, are almost identical to those of the two-cylinder case, see Figs. 6-9. For both the gB and the GN equations, the force on the third cylinder is further reduced, see Figs 12, 14, 16 and 17. As in the two-cylinder case, the maximum force reduction on the third cylinder is greater for the gB equations (F_{max} = 1.42, 30.4% reduction) than for the GN equations (F_{max} = 1.40, 16.2% reduction). The

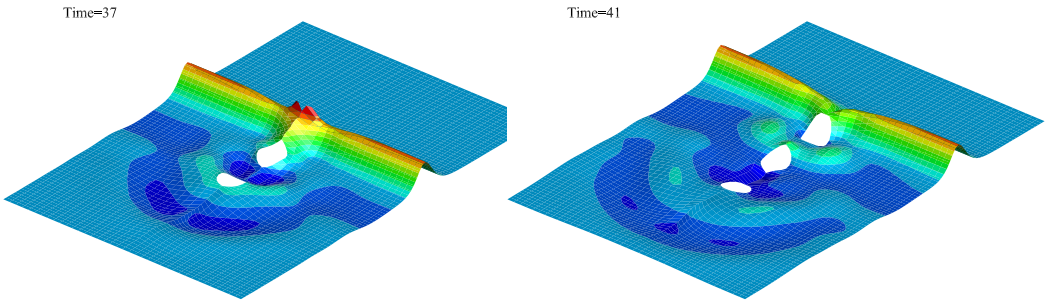

Fig. 10 3-D snapshots of solitary wave surface elevation around three cylinders, calculated by the gB equations, $S = 1.0D, D = 4.0h$ and $H = 0.5h$.

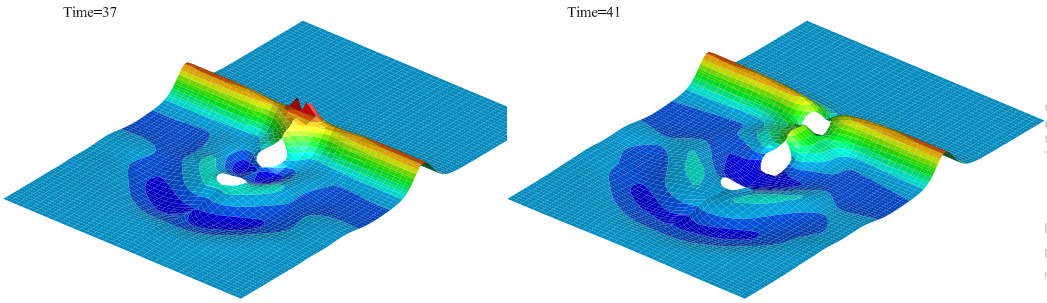

Fig. 11 3-D snapshots of solitary wave surface elevation around three cylinders, calculated by the GN equations, $S = 1.0D, D = 4.0h$ and $H = 0.5h$.

force and moment on the third cylinder, calculated by the gB equations, are similar in value to those of the GN equations. This is the result of the greater single-cylinder force and moment, and the greater force and moment reduction for the gB equations.

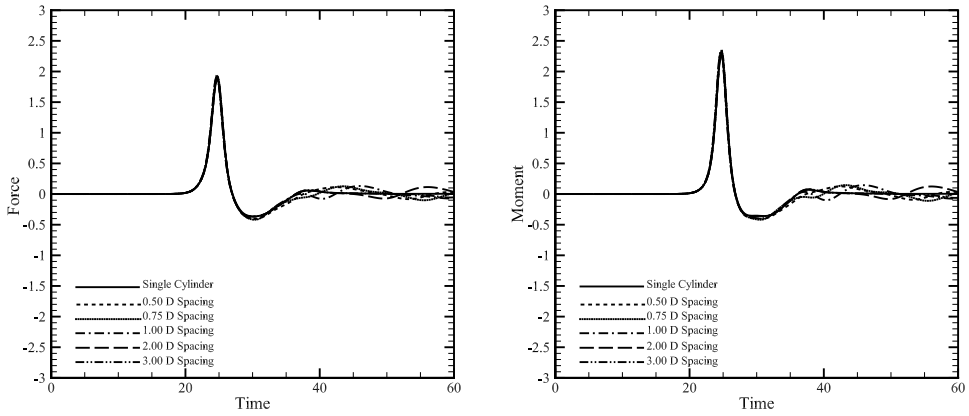

Fig. 12 Solitary wave forces and moments on the first cylinder of the three cylinder case, calculate by the gB equations, $H = 0.5h, D = 4.0h$.

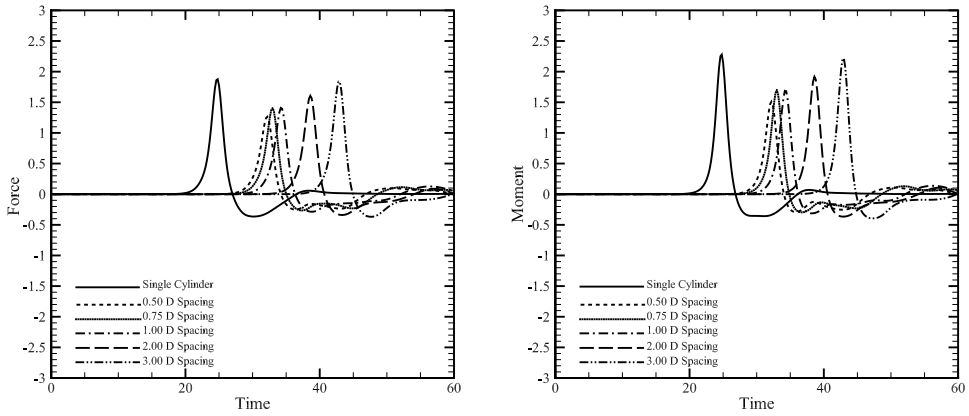

Fig. 13 Solitary wave forces and moments on the second cylinder of the three cylinder case, calculate by the gB equations, $H = 0.5h, D = 4.0h$.

7.4 Further Discussion on Solitary Wave Forces

The maximum forces resulting from solitary waves for the one, two and the three cylinder cases are shown in Figs. 18, 19 and 20. The single cylinder case corresponds to $(S/D) \to \infty$. The maximum force is the maximum absolute value of the horizontal force acting on the individual cylinders. The gB equations, both in this study and in the earlier study of Wang and Jiang (1994),

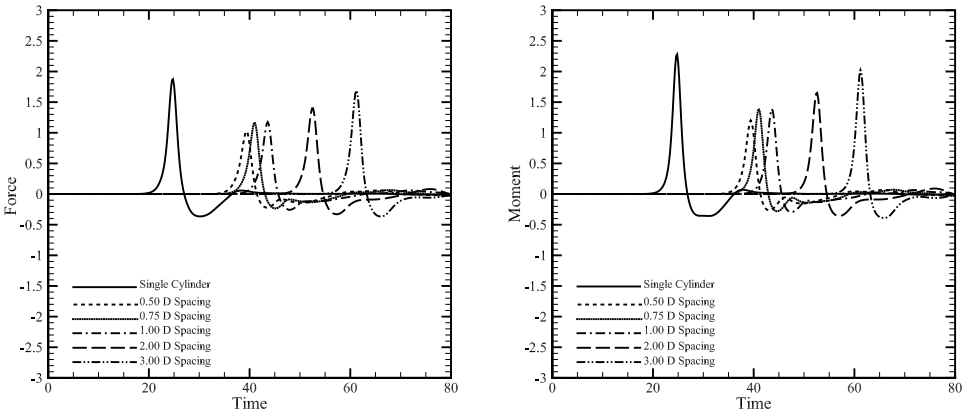

Fig. 14 Solitary wave forces and moments on the third cylinder of the three cylinder case, calculate by the gB equations, $H = 0.5h, D = 4.0h$.

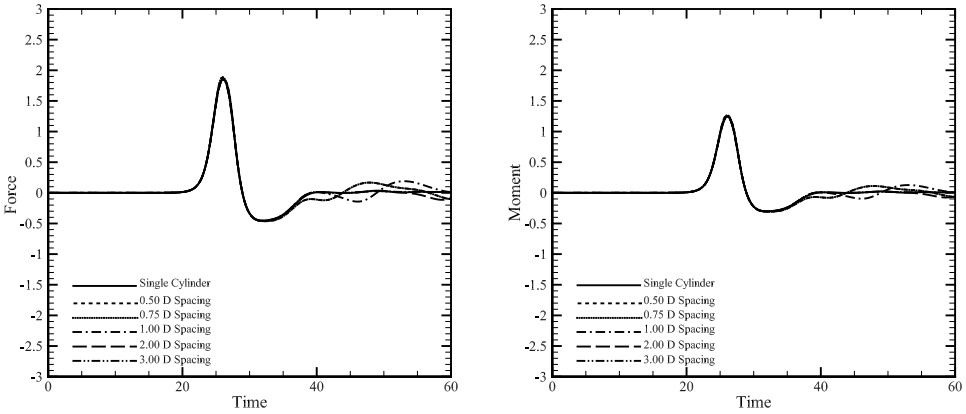

Fig. 15 Solitary wave forces and moments on the first cylinder of the three cylinder case, calculate by the GN equations, $H = 0.5h, D = 4.0h$.

showed that the upwave cylinders effectively shielded the downwave cylinders; see Figs. 19 and 20. The shielding effect is also predicted by the GN equations, however, in smaller magnitude. Since the GN equations are in closer agreement with the experimental data, it is anticipated that the gB equations over-predict the amount of shielding. The closer the cylinders are together, the greater the shielding and the greater the reductions are. The third cylin-

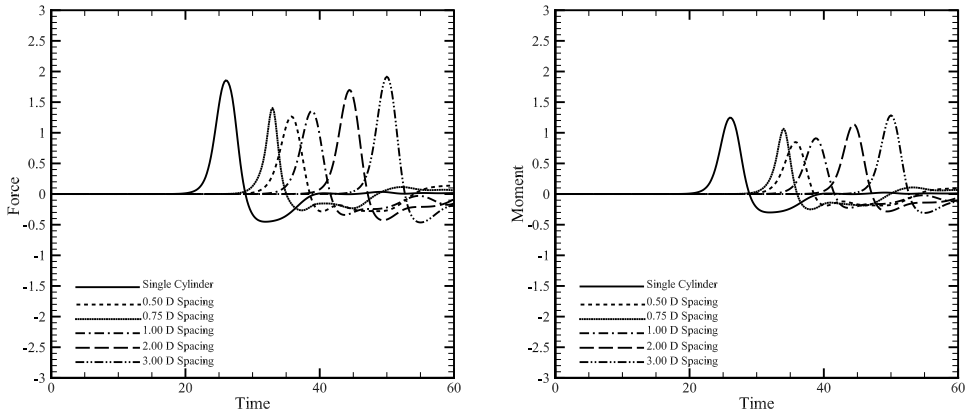

Fig. 16 Solitary wave forces and moments on the second cylinder of the three cylinder case, calculate by the GN equations, $H = 0.5h, D = 4.0h$.

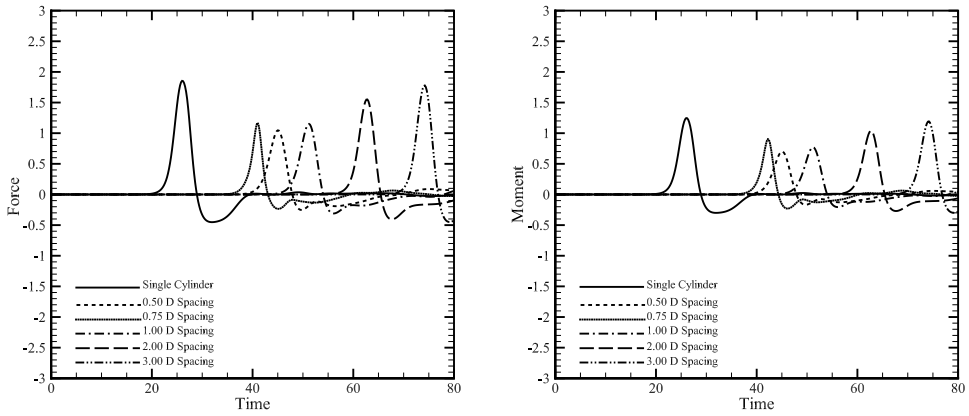

Fig. 17 Solitary wave forces and moments on the third cylinder of the three cylinder case, calculate by the GN equations, $H = 0.5h, D = 4.0h$.

der receives more shielding than the second cylinder. The downwave cylinders have negligible effect on the upwave cylinders.

8 Concluding Remarks

The problem of interaction of solitary waves with multiple in-line fixed, vertical, circular cylinders in shallow water is studied by use of the Green-Naghdi

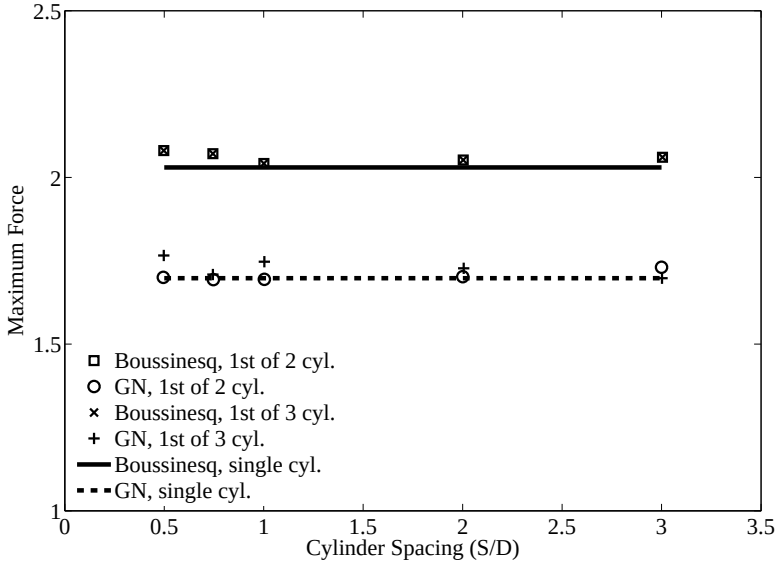

Fig. 18 Solitary wave maximum forces on the first cylinder, for one, two and three cylinders cases, versus cylinder spacing, $H = 0.5h$ and $D = 4.0h$

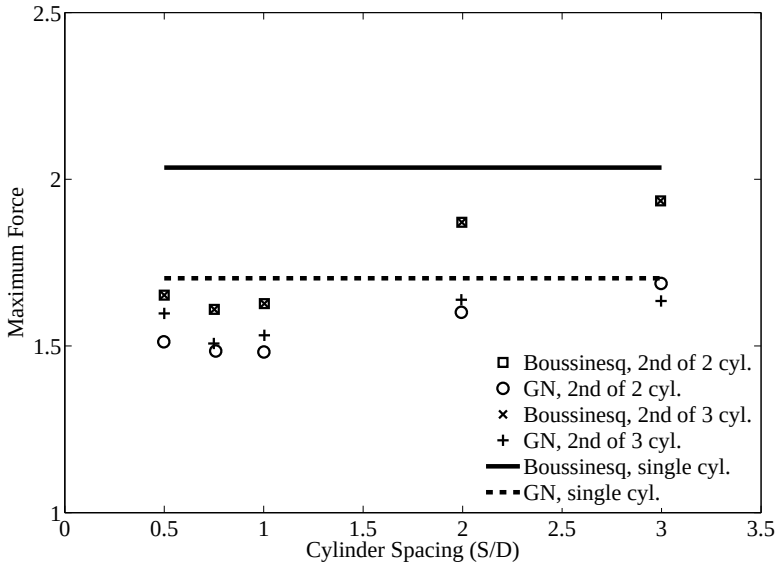

Fig. 19 Solitary wave maximum forces on the second cylinder, for one, two and three cylinders cases, versus cylinder spacing, $H = 0.5h$ and $D = 4.0h$

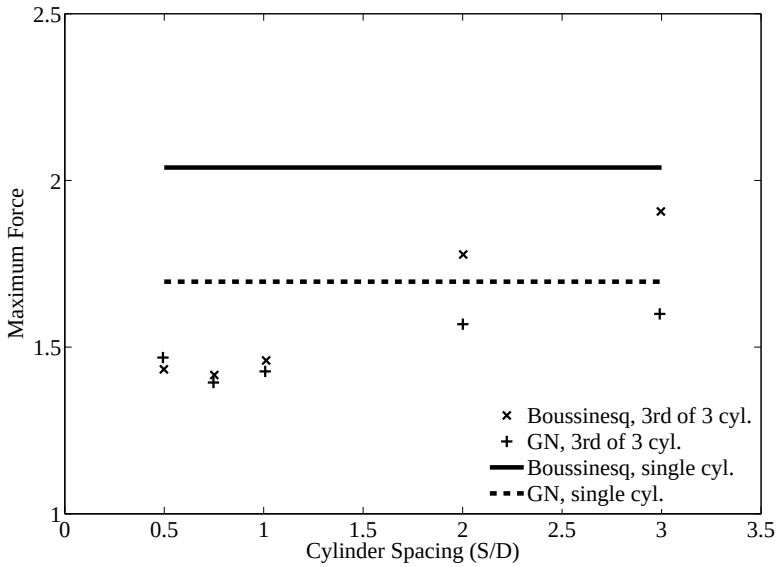

Fig. 20 Solitary wave maximum forces on the third cylinder, for one, two and three cylinders cases, versus cylinder spacing, $H = 0.5h$ and $D = 4.0h$

equations and the Boussinesq equations. The solution is formulated using a boundary-fitted curvilinear coordinate system that allows utilizing a finite-difference method in solving the problem. The wave-induced horizontal force and the overturning moment are obtained by integrating the pressure around the vertical cylinders. In the model developed based on the Green-Naghdi equations, the total pressure distribution around the vertical cylinders is obtained assuming a linear distribution of pressure over the water column. Accuracy and error associated with the numerical calculations can be assessed by monitoring the mass and moment throughout the computations.

Overall, close agreement is observed between the results of the Green-Naghdi equations and the Boussinesq equations with laboratory measurements and existing theoretical solutions. The performance of the Green-Naghdi equations is found to be generally better than the Boussinesq equations. They produce values for the forces and the moments that are in slightly closer agreement with both the experimental data and other predictions. The results of the GN equations and the Boussinesq equations are in closer agreement for smaller cylinder spacings.

It is found that the presence of the second and third cylinders on the wave loads on all cylinders is significant in general. In a number of cases studied here, the resultant loads on the first cylinder has increased due to the second and third cylinders. Such effect is found to be a function of the distance between the cylinders. This is in qualitative agreement with the results obtained for wave interaction with an array of vertical cylinders in deep water. In all cases, however, the first cylinder has provided shielding effect and the maximum forces on the second and third cylinders are smaller than that on the first cylinder. The shielding effect increases as the distance between the cylinders decreases.

The Green-Naghdi equations cannot possess a moment equation, or an equation for the pressure as a function of the water depth that can be used to produce the moment. It is shown in this study that the Green-Naghdi equations can produce accurate predictions of moments when a linear distribution of pressure with depth is assumed. The associated error to this assumption is calculated and found to be negligible. The agreement between the moments calculated through the Green-Naghdi equations and the generalized Boussinesq equations is comparable to the agreement between the forces determined by these methods, and the results are in good agreement with measurements and analysis of laboratory experiments. Note that the assumption of linear pressure variation over depth does not mean that the pressure is hydrostatic.

It is noted that it should be possible to solve the same physical problem by use of higher levels of the GN equations that possess better nonlinearity and dispersive characteristics, however, at a much greater computational effort.

References

Barlas B (2012) Interactions of waves with an array of tandem placed bottom-mounted cylinders. J of Marine Science and Technology 20(1):103–110

Burden RL, Faires JD (1985) Numerical Analysis, 3rd edn. Prindle, Weber & Schmidt Publishers, Boston

Demirbilek Z, Webster WC (1992) Application of the Green-Naghdi theory of fluid sheets to shallow water wave problems. Tech. Rep. CERC-92-11, US Army Corps of Engineers, Vicksburg, Mississippi, 48 p.

Ertekin RC (1984) Soliton generation by moving disturbances in shallow water: Theory, computation and experiment. PhD thesis, Ph.D. Dissertation, University of California at Berkeley, May, v+352 pp.

Ertekin RC (1988) Nonlinear shallow water waves: The Green-Naghdi equations. In: Proc. Pacific Congress on Marine Sci. and Techno., PACON '88, Honolulu, pp OST6/42–52

Ertekin RC, Webster WC, Wehausen JV (1986) Waves caused by a moving disturbance in a shallow channel of finite width. J Fluid Mechanics 169:275–292

Ertekin RC, Qian ZM, Wehausen JV (1990) Upstream Solitons and Wave Resistance, World Scientific, New Jersey. Chapter in Engineering Science, Fluid Dynamics, pp 29–43

Ertekin RC, Hayatdavoodi M, Kim JW (2014) On some solitary and cnoidal wave diffraction solutions of the Green-Naghdi equations. Applied Ocean Research 47:125–137, DOI: 10.1016/j.apor.2014.04.005

Ghadimi P, Bandari HP, Rostami AB (2012) Determination of the heave and pitch motions of a floating cylinder by analytical solution of its diffraction problem and examination of the effects of geometric parameters on its dynamics in regular waves. International Journal of Applied Mathematical Research 1(4):611–633

Green AE, Naghdi PM (1976a) A derivation of equations for wave propagation in water of variable depth. Journal of Fluid Mechanics 78:237–246

Green AE, Naghdi PM (1976b) Directed fluid sheets. Proc of the Royal Society of London Series A, Mathematical and Physical Sciences 347(1651):447–473

Green AE, Naghdi PM (1977) Water waves in a nonhomogeneous incompressible fluid. J Applied Mechanics 44(4):523–528

Green AE, Naghdi PM (1984) A direct theory of viscous flow in channels. Arch for Rat Mech and Analysis 86(1):39–64

718 Han Y, Zhan JM, Su W, Li YS, Zhou Q (2015) Comparison of flow fields
719 induced by fixed and oscillatory vertical cylinders in regular waves using 3D
720 numerical model. Ocean Engineering 106:238–251, DOI 10.1016/j.oceaneng.
721 2015.06.050
722 Havelock TH (1940) The pressure of water waves upon a fixed obstacle on
723 water. Proc Roy Soc London A 175:409–421
724 Hayatdavoodi M, Ertekin RC (2015a) Nonlinear wave loads on a submerged
725 deck by the Green-Naghdi equations. J of Offshore Mechanics and Arctic
726 Engineering 137(1):011,102 (1–9), DOI: 10.1115/1.4028,997
727 Hayatdavoodi M, Ertekin RC (2015b) Wave forces on a submerged horizontal
728 plate. Part I: Theory and modelling. J Fluids and Structures 54(April):566–
729 579, DOI: 10.1016/j.jfluidstructs.2014.12.010
730 Hayatdavoodi M, Ertekin RC (2015c) Wave forces on a submerged horizon-
731 tal plate. Part II: Solitary and cnoidal waves. J Fluids and Structures
732 54(April):580–596, DOI: 10.1016/j.jfluidstructs.2014.12.009
733 Isaacson MQ (1978) Interference effects between large cylinders in waves. Proc
734 10th Offshore Tech Conf, Houston, Vol. I(Paper No. OTC 3069):185–192
735 Isaacson MQ (1983) Solitary wave diffraction around large cylinders. J Wa-
736 terways, Port, Coastal and Ocean Eng 109(1):121–127
737 Isaacson MQ, Cheung KF (1992) Time-domain second-order wave diffraction
738 in three dimensions. J Waterways, Port, Coastal and Ocean Engineering
739 118(5):496–517
740 Kagemoto H, Murai M, Saito M, Molin B, Malenica Š (2002) Experimental
741 and theoretical analysis of the wave decay along a long array of vertical
742 cylinders. J of Fluid Mechanics 456:113–135
743 Kamath A, Alagan Chella M, Bihs H, Arntsen ØA (2015) Evaluating wave
744 forces on groups of three and nine cylinders using a 3D numerical wave tank.
745 Engineering Applications of Computational Fluid Mechanics 9(1):343–354
746 Kudeih M, Cornett A, Nistor I (2010) An experimental study of wave and
747 current-induced forces on a compact linear array of vertical cylinders in
748 shallow water. 32nd Conference on Coastal Engineering, Shanghai, China
749 1(32):10
750 Linton CM, Evans DV (1990) The interaction of waves with arrays of vertical
751 circular cylinders. J Fluid Mechanics 215:549–569
752 MacCamy RC, Fuchs RA (1954) Wave forces on a pile: a diffraction theory.
753 Tech Memo 69, US Army Corps of Engineers

754 Malenica S, Eatock Taylor R, Huang JB (1999) Second-order water wave
755 diffraction by an array of vertical cylinders. Journal of Fluid Mechanics
756 390:349–373, DOI 10.1017/S0022112099005273
757 McIver P, Evans D (1984) Approximation of wave forces on cylinder arrays.
758 Applied Ocean Research 6(2):101–107
759 Mei CC (1989) The Applied Dynamics of Ocean Surface Waves. World Scien-
760 tific, Singapore
761 Mo W (2010) Numerical investigation of solitary wave interaction with group
762 of cylinders. PhD thesis, Cornell University, xvi+169 p.
763 Mo W, Liu PLF (2009) Three dimensional numerical simulations for non-
764 breaking solitary wave interacting with a group of slender vertical cylinders.
765 International Journal of Naval Architecture and Ocean Engineering 1(1):20–
766 28
767 Neill DR (1996) The nonlinear interaction of waves with multiple, vertical, in-
768 line cylinders. Ph.D. Dissertation, Dept. of Ocean Engineering, University
769 of Hawaii
770 Neill DR, Ertekin RC (1997) Diffraction of solitary waves by a vertical cylinder:
771 Green-Naghdi and Boussinesq equations. Proc 16th Int Conf on Offshore
772 Mechanics and Arctic Engineering, OMAE '97, ASME, Yokohama, Japan,
773 I-B:63–71
774 Omer GC, Hall HH (1949) The scattering of a tsunami by a cylindrical island.
775 Bulletin of the Seismological Society of America 39(4):257–260
776 Qian ZM (1988) Numerical grid generation and nonlinear waves generated by
777 a ship in a shallow-water channel. M.S. Thesis, Dept of Ocean Engineering,
778 University of Hawaii, v+121 pp.
779 Qian ZM (1994) Calculations of three dimensional nonlinear ship waves and
780 ship resistance in a shallow water channel. Ph.D. Dissertation, Dept. of
781 Ocean Engineering, University of Hawaii
782 Rayleigh L (1876) On waves. Phil Mag I(5):257–279
783 Roddier D (1994) Diffraction and refraction of solitons around a false wall.
784 M.S. Thesis, Dept. of Ocean Engineering, University of Hawaii
785 Roddier D, Ertekin RC (1999) Diffraction and remodelization of solitons
786 around a false wall. Chaos, Solitons and Fractals 10(7):1221–1240
787 Shapiro R (1975) Linear filtering. Mats Comput 29:1094–1097
788 Shields JJ, Webster WC (1988) On direct methods in water-wave theory. J
789 Fluid Mechanics 197:171–199

Spring BH, Monkmeyer PL (1974) Interaction of plane waves with vertical cylinders. In: Proceedings of the 14th international conference on coastal engineering, Copenhagen, Denmark, vol 107, pp 1828–1845

Teng M, Wu TY (1992) Nonlinear water waves in channels of arbitrary shape. J Fluid Mechanics 242:211–233

Thompson JF, Thames FC, Mastin CW (1977) Boundary-fitted curvilinear system for solutions of partial differential equations on fields containing any number of arbitrary two dimensional bodies. Report No. CR2729, NASA

Wang KH, Jiang L (1994) Interactions of solitary waves with cylinder arrays. In: Proc. 13th Int. Conf. on Offshore Mechanics and Arctic Engineering, ASME, Houston, Texas, USA,, vol I, pp 99–107

Wang KH, Wu TY, Yates GT (1992) Three-dimensional scattering of solitary waves by vertical cylinder. J Waterway, Port, Coastal and Ocean Engineering, 118(5):551–566

Wu D, Wu TY (1982) Three-dimensional nonlinear long waves due to moving surface pressure. In: Proc. 14th Symp. on Naval Hydrodynamics, Washington, D.C., National Academy Press, Washington, D.C., 1983, pp 103–125

Wu TY (1981) Long waves in ocean and coastal waters. J Engineering Mechanics Division 107(3):501–522

Yang C, Ertekin RC (1992) Numerical simulation of nonlinear wave diffraction by a vertical cylinder. J Offshore Mechanics and Arctic Engineering 114(1):36–44

Yates GT, Wang KH (1994) Solitary wave scattering by a vertical cylinder: Experimental study. Proc 4th Int Offshore and Polar Engineering Conference, ISOPE '94, Osaka, Japan, III:118–124

Zhao BB, Duan WY, Ertekin RC (2014a) Application of higher-level GN theory to some wave transformation problems. Coastal Engineering 83:177–189, DOI:10.1016/j.coastaleng.2013.10.010

Zhao BB, Ertekin RC, Duan WY, Hayatdavoodi M (2014b) On the steady solitary-wave solution of the Green–Naghdi equations of different levels. Wave Motion 51(8):1382–1395, DOI:10.1016/j.wavemoti.2014.08.009

Zhao BB, Duan WY, Ertekin RC, Hayatdavoodi M (2015) High-level Green–Naghdi wave models for nonlinear wave transformation in three dimensions. Journal of Ocean Engineering and Marine Energy 1(2):121–132, DOI:10.1007/s40,722–014–0009–8